HYDRODYNAMICS OF AN OSCILLATING WATER COLUMN SEAWATER PUMP PART I: THEORETICAL ASPECTS.

S.P.R. Czitrom[1], R. Godoy[1], E. Prado[1], P. Pérez[1] and R. Peralta-Fabi[2].

Abstract

A wave-driven seawater pump, composed of a resonant and an exhaust duct joined by a variable-volume air compression chamber, is studied. The time dependent form of Bernoulli's equation, adapted to incorporate losses due to friction, vortex formation at the mouths and radiation damping, describes the pump behaviour. A dimensional analysis of the pump equations shows that a proposed scale-model will perform similar to a full-scale seawater pump. Fluid oscillations in the ducts perform similar to a damped, two-mass spring system, excited by the waves. A resonant condition can be maintained, for different wave frequencies, by varying the volume of air in the compression chamber. The dimensional analysis shows that the basic behaviour of the pump is linear and that its' performance can be significantly increased by optimising the design of the duct mouths. Linear estimates of the resonant air chamber volume and flow rate through the pump are derived.

INTRODUCTION

A considerable number of wave energy converters has been developed recently (Evans et al., 1979; McCormick, 1974; Salter, 1974; Isaacs et al., 1976; Tjugen, 1993). A particular class of these devices operates with waves driving an oscillating water column (OWC) which in turn drives electric power turbines (Evans, 1982; Sarmento and Falcao, 1985; Malmo and Reitan, 1985; Masuda, 1971; Budall and Falnes, 1975; Raju, et al., 1994). Most OWC systems take advantage of the amplification that results from resonance at the driving wave frequency to increase power output from the turbines. Out of resonance, phase control mechanisms are used to optimise performance (Justino et al., 1994), although efficiency is significantly reduced, mostly by the conversion between types of energy (e.g. kinetic-electric).

Efficiency in wave energy devices of the OWC type can be substantially increased if the useful end-product energy is of an equivalent type (kinetic-kinetic) and a resonant condition is maintained. In this paper, a wave driven sea water pump, which has potential for various coastal management purposes such as aquaculture, flushing out of contaminated areas or the recovery of isolated coastal lagoons as breeding grounds is described (see also Czitrom, 1996). Apart from avoiding energy type conversions, performance of the pump (based on a design by Carey and Meratla, 1976) is optimised by a novel tuning mechanism (Czitrom, patent pending) that keeps the system at resonance with the driving waves.

In previous papers (Czitrom, 1996; Czitrom et. al, 1997), the equations that describe the system were derived and their validity was tested, by comparing data observed in wave tank

[1] Instituto de Ciencias del Mar y Limnología, Circuito Exterior S/N, Ciudad Universitaria, UNAM, 04510 México D.F., México.
[2] Facultad de Ciencias, Circuito Exterior S/N, Ciudad Universitaria, UNAM, 04510 México D.F., México.

experiments with a scale model of the pump against numerical integrations of the pump equations. These comparisons showed that basically, the equations are well posed although some discrepancies occurred. In this paper, a full derivation of the equations is made and advances in the definition of some of the terms are presented, which substantially improve performance of the numerical model. A dimensional analysis of the pump equations gives insight to the relative importance of the terms, thereby increasing our understanding of the physics involved, and shows that a full scale system will perform similar to the wave tank model of the pump. The revised theoretical aspects of the pump and its hydrodynamics set the stage for a new comparison against the observed wave tank data in Part II of this paper.

A schematic diagram of the seawater pump can be seen in Figure 1. The wave-induced pressure signal at the mouth of the resonant duct drives an oscillating flow that spills water into the compression chamber, and through the exhaust duct to the receiving body of water, with each passing wave. Air in the chamber behaves like a spring against which water in the resonant and exhaust ducts oscillates. Maximum efficiency is attained at resonance when the system natural frequency of oscillation coincides with the frequency of the driving waves (see Lighthill, 1979; Evans, 1982; Falnes & McIver, 1985). A resonant condition can be maintained for different wave frequencies by means of a variable volume compression chamber that adjusts the hardness of the air spring.

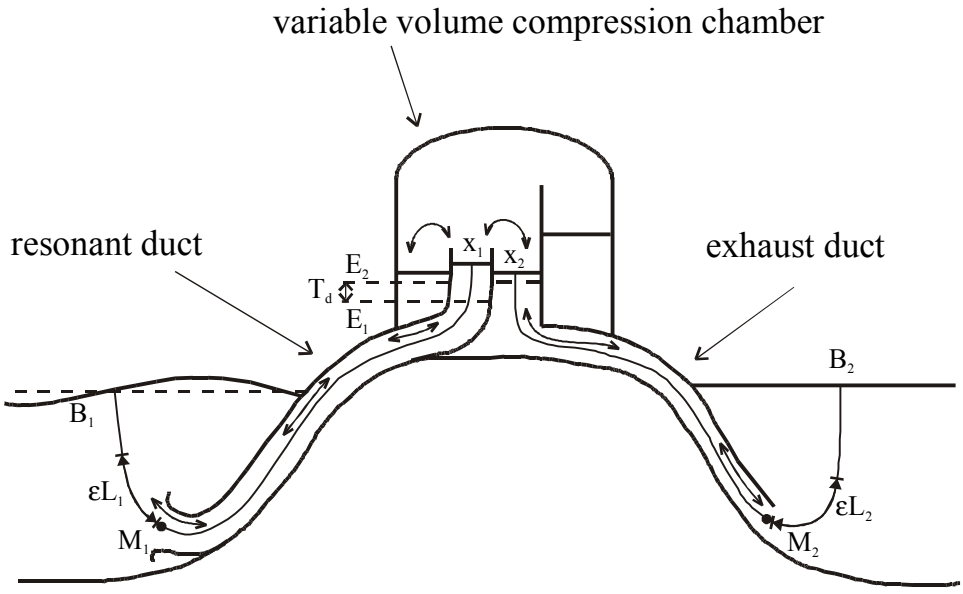

Figure 1. Schematic diagram of the wave driven resonant seawater pump.

SYSTEM EQUATIONS

In the absence of pumping, that is when there is no spilling in the compression chamber, water surface displacement in the resonant and exhaust ducts can be described using equations derived as follows. Referring to Figure 1, the time dependent form of Bernoulli's equation (1) was applied, similar to Knott & Flower (1979), to the stream lines $X_1E_1M_1B_1$ and $X_2E_2M_2B_2$, from the fluid surfaces in the compression chamber, through the resonant and exhaust ducts, to the ocean and receiving water body surfaces respectively. Velocity was considered negligible at B_1 and B_2.

Figure 2 shows a plot of *dV/dt*, used to obtain the integral term in Bernoulli's equation along the exhaust duct streamline (first term in equation 2b). Assuming incompressibility, changes from X_2 to M_2 depend on the area of the section being traversed (A) such that $A\ dV/dt$ is constant along the streamline, at any given time. Outside the duct's mouth, flow dies out at a certain distance, adding to the integral in Bernoulli's equation an amount proportional to *dV/dt* and to the size of the region near the mouth affected by movements in the duct. This region is known as an 'added mass' which we have included in equations 2 by increasing the duct length by a given proportion (ε), in the same way as Knott & Mackley (1980).

$$\int_a^b \partial V/\partial t \cdot ds + \frac{V^2}{2} + \frac{P}{\rho} + gX = Const. \tag{1}$$

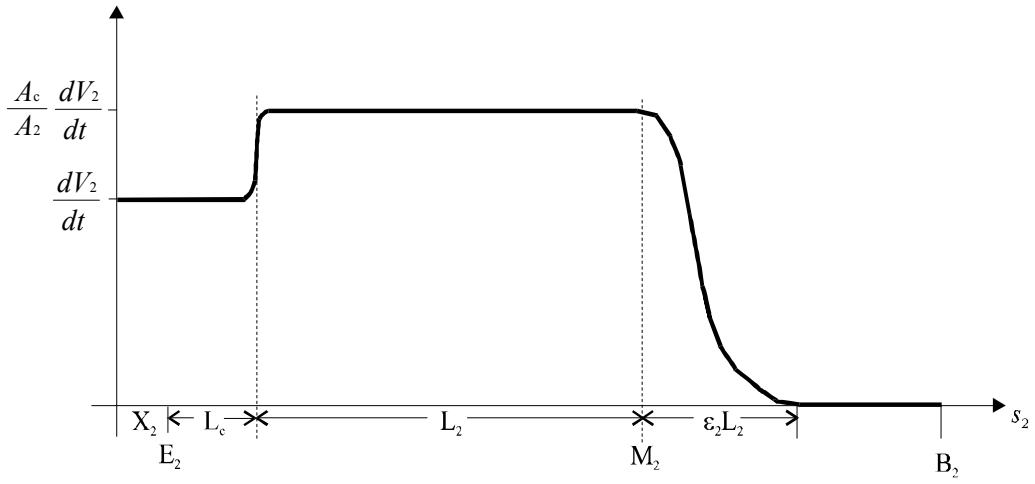

Figure 2. *dV/dt* along the streamline $X_2E_2M_2B_2$ shown in Figure 1.

$$(X_1 + L_1(1+\varepsilon_1) + T_d/\cos\theta)\ddot{X}_1 + \frac{\dot{X}_1^2}{2} + \left(\frac{K_1}{2} + \frac{(L_1 + T_d/\cos\theta)}{D_1} f_1 + C_{r1}\right)\dot{X}_1\left|\dot{X}_1\right| + \\ + \frac{(P_A - \rho gH)}{\rho}\left[\left(1 - \frac{A_1X_1}{V_o} - \frac{A_cX_2}{V_o}\right)^{-\gamma} - 1\right] + g\cdot\cos\theta\cdot X_1 = W/\rho, \tag{2a}$$

$$(X_2 + \frac{A_c}{A_2}L_2(1+\varepsilon_2) + L_c)\ddot{X}_2 + \frac{\dot{X}_2^2}{2} + \left(\frac{K_2}{2} + \frac{L_2}{D_2}f_2 + C_{r2}\right)\left(\frac{A_c}{A_2}\right)^2\dot{X}_2\left|\dot{X}_2\right| + \\ + \frac{(P_A - \rho gH)}{\rho}\left[\left(1 - \frac{A_1X_1}{V_o} - \frac{A_cX_2}{V_o}\right)^{-\gamma} - 1\right] + gX_2 = 0\cdot \tag{2b}$$

The second and fifth terms in equations 2 come directly from Bernoulli's equation. Coupling of the two equations occurs through the air compression term (4th in both equations), which was obtained assuming adiabatic conditions. External forcing by the waves is added on the right hand side of the equation for the resonant duct (2a).

Subscripts 1, 2 and c in equations (2) correspond to the resonant and exhaust ducts and compression chamber respectively. X is the surface displacement, in either duct, relative to its' equilibrium position in the compression chamber, and L, D and A are lengths, diameters and areas respectively. L_1 (the resonant duct length) and T_d (the tidal height) are referred to the equilibrium position on the exhaust duct side of the compression chamber (E_2). In addition:

P_A	Atmospheric pressure (kg m^{-1} s^{-2})
ρ	Sea water density (kg m^{-3})
$\gamma = C_p/C_v$	Air compressibility = 1.4
W	Wave pressure signal (kg m^{-1} s^{-2})
T_d	Height of sea level above receiving body of water (includes tidal signal) (m)
Vo	Compression chamber volume (m^3)
H	Height of compression chamber equilibrium position above receiving body of water (m)
ε	Fractional added length due to edge effects at the duct mouth
θ	Resonant duct inclination at the compression chamber
$g' = g\cos\theta$	Reduced gravity due to inclination of the resonant duct at the compression chamber (m s^{-2})
f	Friction loss coefficient for oscillating flow in pipes.
K	Vortex formation energy loss coefficient (see Knott & Mackley, 1980)
C_r	Radiation damping coefficient (see Knott & Flower, 1980).

Expressions were added in equations (2) to account for losses due to vortex ring formation at the duct mouths, friction against the walls and radiation damping due to surface wave generation by oscillations in the ducts (3rd term in both equations). Adding terms to Bernoulli's equation, which deals with inviscid flow, to account for these losses, is an approach which has been used previously under similar conditions with success (see Knott & Flower (1979); Knott & Mackley, 1980; Czitrom et al., 1996). The form given to the third term in equations 1a and 1b was derived assuming that friction, vortex generation and radiation damping can be suitably represented as pressure losses, in a fashion similar to that used in hydraulics to represent friction in unidirectional pipe flow.

Using dimensional analysis, and assuming that the pressure loss due to the formation of vortex rings at the duct mouths is a function of the duct diameter D, the oscillation frequency Ω, the oscillation velocity V ($\equiv \dot{X}$) and the amplitude of the velocity of oscillation V_{max}, as well as the kinematic viscosity ($\nu = \rho/\mu$), we obtain

$$\frac{\Delta P}{\rho} = V^2 K\left(\frac{DV_{max}}{\nu}, \frac{\Omega D^2}{\nu}, \frac{V}{V_{max}}\right). \tag{3}$$

The loss of pressure due to friction (Czitrom, 1996) can be written as

$$\frac{\Delta P}{\rho} = V^2 f\left(\frac{L}{D}, \frac{DV_{max}}{\nu}, \frac{\Omega D^2}{\nu}, \frac{V}{V_{max}}, \frac{r}{D}\right), \tag{4}$$

if we assume that it will be a function of the above variables as well as the duct length L and the wall roughness r. The non-dimensional number L/D can be taken out of the parenthesis if it is assumed, quite reasonably, that the total loss of pressure due to friction must be proportional to the duct's length. Both equations (3) and (4) exhibit a dependence on a conventional Reynolds number, a modified (or oscillating) Reynolds number and a non-dimensional velocity.

Radiation damping, on the other hand, is assumed to depend on the duct's diameter, the oscillation frequency, velocity and velocity amplitude, giving

$$\frac{\Delta P}{\rho} = V^2 C_r\left(\frac{D\Omega}{V_{max}}, \frac{V}{V_{max}}\right). \tag{5}$$

The actual forms used for K, f, and C_r in equations (3), (4) and (5) are discussed later in this section.

At the time of pumping, fluid surges from the resonant duct, and spills into the exhaust side of the compression chamber. The fluid surface above the resonant duct bulges upward inducing a back pressure on the fluid in the duct, which we assume proportional to the bulge height ϕ. Using dimensional analysis and assuming that ϕ must be a function of the duct's diameter D, the instantaneous water velocity V as it surges from the duct, the kinematic viscosity v and the surface tension coefficient ζ,

$$\phi = Df'\left(\frac{DV}{v}, \frac{V^2}{gD}, \frac{\rho DV^2}{\zeta}\right). \tag{6}$$

A series of experiments were carried out using vertical tubes with various diameters connected to a variable flow tap. Water height at the centre of the bulge was measured for each set of experimental conditions to obtain a relation between the height and the Reynolds, Froude and Weber numbers (1st, 2nd and 3rd respectively in expression 6). It was found that, given the experimental conditions ($2\,700 < \mathrm{Re} < 22\,700$, $0.1 < \mathrm{Fr} < 4.8$, $5.8 < \mathrm{We} < 219.8$), the only relevant variable was the Froude number such that

$$\phi = DFr^{0.635}, \tag{7}$$

explains 96.8 % of the variance in the experimental data.

That the Weber number, which compares inertial and surface tension forces, is not important, is reasonable considering that surface tension becomes relevant for We ~ 1. The dominance of the Froude number shows that the attainable height in a vertical jet is essentially a balance between the inertial and the gravitational forces. The irrelevance of Re shows that this height is not affected by the balance between the inertial and the viscous forces over a wide range of experimental conditions.

Approximating 0.635 with 2/3 and rearranging,

$$\phi = \sqrt[3]{DV^4/g^2} \tag{8}$$

is obtained. This expression is used in the following deduction of the equations that govern fluid motion in the ducts during pumping.

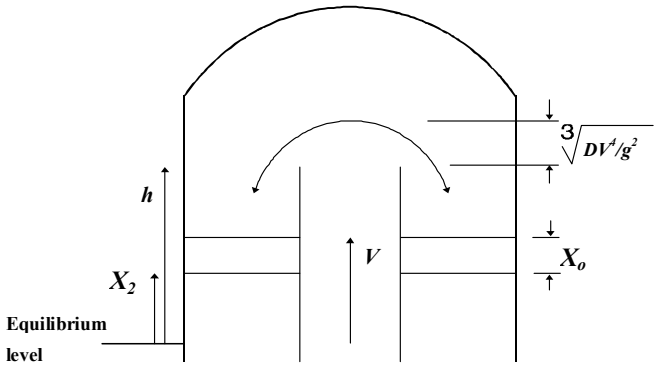

Figure 3. Interior of the compression chamber during spilling.

Applying Bernoulli's equation in a similar fashion for the case of pumping, and referring to Figure 3, equations for the resonant and exhaust ducts during spilling in the compression chamber were derived:

$$\left[\frac{(h+\phi/2)}{\cos\theta} + L_1(1+\varepsilon_1)\right]\dot{V} + \frac{1}{2}\left(\frac{d\phi}{dt}\right)^2 + \left(\frac{K_1}{2} + \frac{(L_1 + h/\cos\theta)}{D_1} f_1 + C_{r1}\right)V|V| + \\ + \frac{(P_A - \rho g H)}{\rho}\left[\left(1 - \frac{A_1}{V_o}\left(\frac{h - T_d + \phi}{\cos\theta}\right) - \frac{A_c}{V_o}(X_2 + X_0)\right)^{-\gamma} - 1\right] + g'\left(\frac{h - T_d + \phi}{\cos\theta}\right) = W/\rho, \tag{9a}$$

$$\left[X_2 + X_0 + L_2\frac{A_c}{A_2}(1+\varepsilon_2) + L_c\right]\ddot{X}_2 + \frac{\left(\dot{X}_2 + \dot{X}_0\right)^2}{2} + \left(\frac{K_2}{2} + \frac{L_2}{D_2} f_2 + C_{r2}\right)\left(\frac{A_c}{A_2}\right)^2 \dot{X}_2\left|\dot{X}_2\right| + \\ + \frac{(P_A - \rho g H)}{\rho}\left[\left(1 - \frac{A_1}{V_o}\frac{(h - T_d + \phi)}{\cos\theta} - \frac{A_c}{V_o}(X_2 + X_0)\right)^{-\gamma} - 1\right] + g(X_2 + X_0) = 0. \tag{9b}$$

Here h is the resonant duct sill height above the equilibrium position in the compression chamber and

$$X_0 = \frac{A_1}{A_c}\int_{t_0}^{t} V dt$$

is the change in water level in the exhaust side of the compression chamber which results from spilling. For each cycle, t_0 is the time at which spilling commences.

In deducing equations (9), only the $\phi/2$ in the first term of (9a) needs further comment. Referring to Figure 2, the equivalent plot of dV/dt for the resonant duct during pumping must start near zero at the origin, which corresponds to the top of the bulge created by spilling, up to full value at the resonant duct sill. The contribution to the integral in Bernoulli's equation of this section of the path can be approximated with the area of a triangle, thus explaining the $\phi/2$.

Equation 9a for the resonant duct is now written in terms of the fluid velocity (rather than the surface displacement as in equation 2a) because the position of the surface above the resonant duct sill, as water is being spilt, no longer represents water displacement within the duct.

Equations (2) and (9) include a series of non-linear terms which make analytic solutions quite difficult to visualise. This is particularly true of equations (9) which describe the pumping half of the cycle. In Part II of this paper we resort to numerical methods to integrate these equations and compare the results to experimental data obtained with a scale model of the pump.

Integration of equations (2) and (9) requires providing appropriate expressions for f, K and C_r in the terms for pressure loss due to friction, vortex formation and radiation damping respectively (see equations 3, 4 and 5). Considering friction loss first, the appropriate form for this term must depend on the type of flow –laminar, transitional or turbulent– present in the duct, similar to a Moody diagram for unidirectional flow in pipes. White (1991) showed that a modified Reynolds number for oscillating flow (Rem = $\Omega D^2/4\nu$, where D is the pipe diameter), characterises the nature of the observed flow (see also Ohmi et al., 1980; Ohmi & Iguchi, 1980a and b). Laminar conditions are present for Rem < 2000 while a transition to turbulent flow might occur for Rem's greater than this threshold and on to fully turbulent flow at very large Rem's.

In the wave tank experiments described in Part II of this paper, Rem ≅ 2000, which is at the limit of laminar oscillating flow. Water movement in the ducts indeed appeared non-turbulent when Kaleiroscope fluid was pumped through the system. Laminar flow in pipes, driven by a sinusoidal pressure gradient, has been studied by various authors (Sexl, 1930, Uchida, 1956, Rott, 1964). For very low Rem's (< 1), viscosity dominates inertial forces and the velocity profile is nearly a Poiseuille flow in phase with the driving pressure gradient. For greater Rem's (higher frequencies or larger duct diameters), a central core of fluid increasingly de-couples from the pressure gradient until it lags behind by $\pi/2$ for Rem > 40. For even greater Rem's, the inertia dominated core region expands and viscous effects increasingly confine themselves to the near wall region where a ring of fluid, called Richardson's annulus, keeps in phase with the pressure gradient (for Rem = 2000, the central core covers 90 % of the duct area). At times of near rest, this ring surges forward in advance of the core so that a pressure drop due to friction occurs even when the sectionally averaged velocity is nil.

Pérez et al. (1996), developed a model for this type of flow. They studied a fluid of density ρ and dynamic viscosity ν in an infinite circular cylinder of radius $D/2$, driven by a pressure gradient that oscillates in time with frequency Ω. Assuming laminar flow, the following solution is found for the corresponding Navier-Stokes equations in cylindrical coordinates:

$$\mathbf{V}(R,T) = \mathbf{k}\frac{P_0}{\rho\omega}\left[P(R)\cos\tau + I(R)\sin\tau\right].$$

Here $R = 2r/D$ is a dimensionless radial coordinate, $\tau = \Omega t$ is a dimensionless time, P_0 is the amplitude of the pressure gradient, **k** is the unit vector along the cylinder axis,

$$P(R) = A\,\mathrm{ber}(R\sqrt{\mathrm{Re}\,m}) - B\,\mathrm{bei}(R\sqrt{\mathrm{Re}\,m}),$$

$$I(R) = 1 - B\,\mathrm{ber}(R\sqrt{\mathrm{Re}\,m}) + A\,\mathrm{bei}(R\sqrt{\mathrm{Re}\,m}),$$

$$A = \frac{\mathrm{bei}(\sqrt{\mathrm{Re}\,m})}{\mathrm{ber}^2(\sqrt{\mathrm{Re}\,m}) + \mathrm{bei}^2(\sqrt{\mathrm{Re}\,m})},$$

and

$$B = \frac{\mathrm{ber}(\sqrt{\mathrm{Re}\,m})}{\mathrm{ber}^2(\sqrt{\mathrm{Re}\,m}) + \mathrm{bei}^2(\sqrt{\mathrm{Re}\,m})}.$$

Here ber(x) and bei(x) are Kelvin functions of zeroth order (Abramowitz & Stegun, 1972). It can be seen that a dependence on the modified Reynolds number Rem appears consistently throughout this solution.

The sectionally averaged velocity in this type of flow is given by

$$V(t) = \frac{P_0}{\Omega\rho}\sqrt{\frac{2}{\mathrm{Re}\,m}}\left[V_1(\mathrm{Re}\,m)\cos\tau + V_2(\mathrm{Re}\,m)\sin\tau\right] \tag{10}$$

where

$$V_1(\mathrm{Re}\,m) = (B-A)\mathrm{ber}_1(\sqrt{\mathrm{Re}\,m}) + (A+B)\mathrm{bei}_1(\sqrt{\mathrm{Re}\,m})$$

and

$$V_2(\mathrm{Re}\,m) = \sqrt{\frac{\mathrm{Re}\,m}{2}} + (A+B)\mathrm{ber}_1(\sqrt{\mathrm{Re}\,m}) + (A-B)\mathrm{bei}_1(\sqrt{\mathrm{Re}\,m}).$$

The pressure drop due to friction can be obtained by equating the expression for the shear stress, estimated at the duct wall, to the pressure gradient needed for balance:

$$\Delta P(t) = LP_0\sqrt{\frac{2}{\mathrm{Re}\,m}}\left[E_1(\mathrm{Re}\,m)\cos t + E_2(\mathrm{Re}\,m)\sin t\right], \tag{11}$$

where

$$E_1(\mathrm{Re}\,m) = (A+B)\mathrm{ber}_1(\sqrt{\mathrm{Re}\,m}) + (A-B)\mathrm{bei}_1(\sqrt{\mathrm{Re}\,m}),$$

$$E_2(\mathrm{Re}\,m) = (A-B)\mathrm{ber}_1(\sqrt{\mathrm{Re}\,m}) - (A+B)\mathrm{bei}_1(\sqrt{\mathrm{Re}\,m}),$$

and bei_1 and ber_1 are Kelvin functions of the first order (Abramowitz & Stegun, 1972; Pérez et. al, 1996).

For the experimental conditions described in Part II of this paper (see also Table 1), $V_1 << V_2$ so that $\Delta P/\rho$ can be expressed as a function of V:

$$\frac{\Delta P}{\rho} = \frac{\Omega L}{V_2}\left[E_2 V \pm E_1 \sqrt{\frac{2}{\mathrm{Re}\, m}\left(\frac{V_2 P_0}{\Omega \rho}\right)^2 - V^2} \right], \tag{12}$$

where the plus sign is used when $dV / dt > 0$. During integration of the numerical model (see Part II of this paper), the oscillating velocity amplitude in the previous cycle was used to compute P_0, the driving pressure gradient amplitude, so that (12) remained real and continuous throughout the new cycle.

Additionally, as a result of the pumping action, there is an average flow through the system so that velocities can be separated into an oscillating and a residual component. Friction losses can be computed using equation (12) for the oscillating component and the known pressure loss for unidirectional laminar flow in pipes for the residual part (64/Re). When plotted against V, equation (12) describes an ellipse centred at the origin, with its major axis inclined with respect to the horizontal. The effect of Richardson's annulus is most clearly apparent at low velocities when a pressure drop due to friction persists despite the absence of motion.

We have derived an expression for pressure losses due to friction in laminar oscillating flow, applicable to the laboratory conditions described in Part II of this paper. For a full-scale oceanic application of the seawater pump, however, the Reynolds (DV_{max}/ν) and the modified Reynolds ($D^2\Omega/4\nu$) numbers acquire values characteristic of turbulent flow (~ 590,000 and ~ 205,000 respectively, using values shown on Table 1). These values are in sharp contrast to those encountered in the laboratory model (7,820 and 2,190, respectively), and we must therefore obtain an expression for frictional losses in fully turbulent oscillatory flow applicable to oceanic conditions. Jonsson (1980) recommended using 10 times the friction factor for fully turbulent unidirectional flow [$f = 10\ (1.14\text{-}2\ \mathrm{Log}_{10}(r/D))^{-2}$], as a good approximation for losses in turbulent oscillatory flow in ducts with very rough walls. This computation can be considered an upper bound to the losses expected in ducts with smooth walls, such as will be used in the seawater pump. We are unaware of a more precise evaluation of this term and it is clear that further work must be carried out for a better definition.

At this point, only K and C_r remain to be determined to complete the equations that describe the system. For the laboratory experimental conditions described in Part II of this paper, these were determined by adjusting them as a unit ($K/2 + C_r$) so that a numerical integration of the pump equations coincided as closely as possible to the observed data. This value was used for the laboratory conditions in the following section. C_r in full-scale oceanic conditions is probably close to the value obtained in the laboratory since the Strouhal number (refer to equation 5 and Table 1) in both situations is very similar (1.12 for the laboratory and 1 for the ocean). K, however, involves quite different Re and Rem numbers as pointed out previously, and it is quite

possible that vortex losses will differ substantially in both situations. Further experimental work needs to be carried out to determine K under oceanic conditions.

DIMENSIONAL ANALYSIS

In order to examine the contribution of each term in the system equations 2a and 2b, for oceanic and laboratory conditions, we rewrote them (equations 13) defining the non-dimensional variables $X = aA_f\chi$ and $t = (T/2\pi)\tau = \Omega^{-1}\tau$ to scale length and time respectively. Here a is the wave amplitude, A_f is the wave size amplification factor within the duct and T is the wave period. The following relation between A_{f1} and A_{f2}, for the resonant and exhaust ducts, was derived assuming momentum conservation for both ducts as a system, and used in equations (13):

$$A_{f2} = \frac{L_1 A_1}{L_2 A_c} A_{f1}.$$

Developing the compression chamber term to third order equations (2) become,

$$\Lambda_1 \ddot{\chi}_1 + \frac{A_{f1}}{2}\dot{\chi}_1^{\,2} + \left(\frac{K}{2} + C_r + \frac{L_1}{D_1} f\right)_1 A_{f1}\dot{\chi}_1\left|\dot{\chi}_1\right| + \mathrm{K}\left[\left(\chi_1 + \frac{L_1}{L_2}\chi_2\right) + \mathrm{K}'\left(\chi_1 + \frac{L_1}{L_2}\chi_2\right)^2 + \mathrm{K}''\left(\chi_1 + \frac{L_1}{L_2}\chi_2\right)^3 + \ldots\right] + \Gamma_1\chi_1 = \Delta Cos(\tau), \quad (13a)$$

$$\Lambda_2 \ddot{\chi}_2 + \mathrm{Z}_1^{\,2}\frac{A_{f1}}{2}\dot{\chi}_2^{\,2} + \left(\frac{K}{2} + C_r + \frac{L_2}{D_2} f\right)_2 \mathrm{Z}_2^{\,2} A_{f1}\dot{\chi}_2\left|\dot{\chi}_2\right| + \mathrm{K}\left[\left(\chi_1 + \frac{L_1}{L_2}\chi_2\right) + \mathrm{K}'\left(\chi_1 + \frac{L_1}{L_2}\chi_2\right)^2 + \mathrm{K}''\left(\chi_1 + \frac{L_1}{L_2}\chi_2\right)^3 + \ldots\right] + \Gamma_2\chi_2 = 0. \quad (13b)$$

Here

$$\Lambda_1 = \left(\frac{L_1(1+\varepsilon)}{a} + \frac{T_d}{aCos\theta}\right), \quad \Lambda_2 = \frac{L_1(1+\varepsilon)}{a}\frac{A_1}{A_2}, \quad \mathrm{K} = \frac{(P_A - \rho g H)\gamma A_1}{\rho a\Omega^2 V_0}, \quad \mathrm{K}' = \frac{(\gamma+1)aA_1A_{f1}}{2V_0},$$

$$\mathrm{K}'' = \frac{(\gamma+1)(\gamma+2)a^2A_1^{\,2}A_{f1}^{\,2}}{6V_0^{\,2}}, \quad \Gamma_1 = \frac{g\cos\theta}{a\Omega^2}, \quad \Gamma_2 = \frac{g}{a\Omega^2}\frac{L_1A_1}{L_2A_c}, \quad \mathrm{Z}_1 = \frac{L_1A_1}{L_2A_c}, \quad \mathrm{Z}_2 = \frac{L_1A_1}{L_2A_2},$$

and

$$\Delta = \frac{g}{a\Omega^2 A_{f1}}.$$

This form of the pump equations was used, in conjunction with the values in Table 1, to estimate the contribution of each term under full-scale oceanic conditions and in the laboratory scale model. Based on the observations and on the numerical model runs, it was assumed that,

under resonant conditions, in the laboratory the resonant duct amplifies the wave signal (A_{fl}) by approximately 4. For oceanic conditions, an amplification of 2 at resonance was assumed. Also, for want of a better suggestion, we took the same values of K obtained under laboratory conditions for vortex losses in the ocean (see Part II of this paper and the previous section), in the understanding that a more appropriate evaluation should be made.

Table 1. Parameters for the laboratory and the ocean used to calculate values on Table 2.

	Lab.	Ocean		Lab.	Ocean		Lab.	Ocean		Lab.	Ocean
L_1	4.08 m	80 m	D_1	0.056 m	1.4 m	$(K/2+C_r)_1$	5	5	r_1		0.01 m
L_2	15 m	70 m	D_2	0.036 m	1.4 m	$(K/2+C_r)_2$	5	5	r_2		0.01 m
V_0	.0134 m	46.8 m^3	H	1.26 m	2 m	D_c	0.14 m	4 m	A_{fl}	4	2
T	2.25 s	15 s	a	0.05 m	0.5 m	ε	0.06	0.06	θ	0	0

For friction in the laboratory model, the non-dimensional form of equation (12) was developed to fourth order giving:

$$\Sigma_i \frac{A_{fi}\Omega L_i}{V_{2i}}\left[E_{2i}\Sigma_i' \dot{\chi}_i \pm E_{1i}\left(1-\left(\Sigma_i' \dot{\chi}_i\right)^2-\left(\Sigma_i' \dot{\chi}_i\right)^4-\cdots\right)\right] \quad \text{(with the + sign when } \ddot{\chi} \geq 0\text{)},$$

Here,

$$\Sigma_i = \frac{2}{\mathrm{Re}\, m_i}\left(\frac{V_{2i}P_{0i}}{\Omega\rho}\right)^2 \text{ and } \Sigma_i' = \frac{aA_{fi}\Omega}{\Sigma_i}.$$

Table 2. Estimates of the size of the various terms in the pump equations 13a and b, when there is no flow through the system, for conditions in the laboratory and in the ocean.

	Laboratory		**Ocean**	
Term	**Resonant**	**Exhaust**	**Resonant**	**Exhaust**
Inertia* (Λ/K) *(Linear)	**1.44**	**3.49**	**3.95**	**3.95**
Velocity squared* (A_{fl}/2K) *(non-linear)	**0.03**	**0.00**	**0.05**	**0.00**
Vortexes & Radiation Damping* ($K/2+C_r)A_{fl}$/K *(non-linear)	**0.34**	**0.14**	**0.23**	**0.30**
***Friction in the Laboratory (Linear)* (ΣΣ'/K)**	**0.01**	**0.00**		
***(Constant)* (Σ/K)**	**0.01**	**0.00**		
***(First non-linear)* (Σ/2K)**	**0.01**	**0.00**		
***(Second non-linear)* (Σ/8K)**	**0.00**	**0.00**		
Friction in the ocean (non-linear)			**0.87**	**0.99**
CompressionChamber* (K/K) *(Linear)	**1.00**	**1.00**	**1.00**	**1.00**
***(First non-linear)* (K')**	**0.04**	**0.04**	**0.04**	**0.04**
***(Second non-linear)* (K'')**	**0.00**	**0.00**	**0.00**	**0.00**
Gravity* (Γ/K) *(Linear)	**0.43**	**0.02**	**2.61**	**0.41**
***Wave forcing* (Δ/K)**	**0.11**		**1.30**	

In Table 2, estimates for the various terms in equations (13a) and (13b) are shown for laboratory and oceanic conditions. Values have been divided throughout by the linear component of the air compression chamber term, since it is the same for the resonant and exhaust ducts, in order to make all terms comparable.

It is clear from Table 2 that the balance of terms for the laboratory and for oceanic conditions is quite similar, so that we can expect the full-scale seawater pump to behave much like the laboratory model. It is also apparent that the linear terms dominate the pump behaviour while the non-linear terms make relatively small contributions. Of the latter, losses due to vortex formation and radiation damping make the largest contributions while friction is relatively small. It is worth recalling that the friction term for oceanic conditions was estimated for fully turbulent oscillatory flow in ducts with very rough walls, and it is likely that this term will be much smaller for the smooth ducts to be used in the full scale pump.

In the absence of losses, water oscillations in the pump at resonance would increase indefinitely. The main role of losses is therefore to limit oscillations in the pump and thus, also it's flow rate. There can be little control over losses due to friction and radiation damping. Vortex formation on the other hand, strongly depends on the shape of the duct mouths (Knott & Flower, 1980). The relatively large size of this term in Table 2 shows that it is worthwhile optimising the shape of the mouth to diminish vortex formation. In Part II of this paper it is shown that a 10 % flow rate increase was observed in the model wave tank experiments, when a crude diffuser was fit to the resonant duct mouth. Further work is being carried out to optimise the design of the duct mouth to minimise losses due to vortex formation.

BASIC BEHAVIOUR OF THE PUMP

The previous analysis shows that, in the absence of spilling in the compression chamber, the wave driven seawater pump can be represented by two masses, two springs and two non-linear dampers coupled as shown in figure 4. The spring on the left represents gravity in the resonant duct, L_1 and L_2 represent the resonant and exhaust duct masses, respectively, and the spring in the middle represents the air compression chamber. The pistons represent the non-linear losses due to friction, vortex formation and radiation damping in the resonant and exhaust ducts.

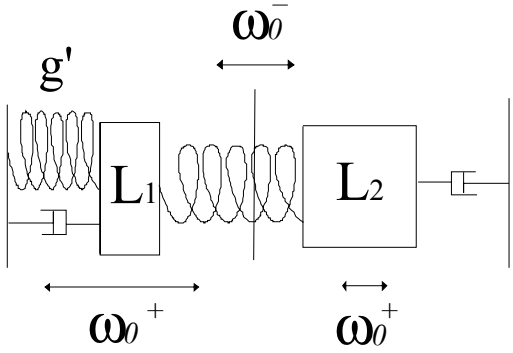

Figure 4. Representation of the model pump as a damped, two mass, spring oscillator.

Neglecting the non-linear terms, while not substantially affecting the general balance of the equations, allows for analytic solutions. As will be shown, this simplification provides additional insight to the system within the limits imposed by the approximation. Assuming a driving wave signal $W = \rho\ a\ g\ \sin(\Omega\ t)$, where a is the surface wave amplitude, and separating variables, equations (2a) and (2b) reduce to a set of two fourth order differential equations:

$$\frac{d^4 X_i}{dt^4} + a_1 \frac{d^2 X_i}{dt^2} + a_2 X_i = a_{3i} \sin(\Omega t),$$

where i=1 and 2 for the resonant and exhaust ducts respectively,

$$a_1 = \frac{g' + \alpha A_1}{L_1'} + \frac{\alpha A_c}{L_2'}, \quad a_2 = \frac{g' \alpha A_c}{L_1' L_2'},$$

$$L_1' = L_1(1+\varepsilon_1) + T_d / \cos\theta, \quad L_2' = L_2(1+\varepsilon_1)\frac{A_c}{A_2},$$

$$a_{31} = \frac{ga(\alpha A_c - L_2' \Omega^2)}{L_1' L_2'}, \quad a_{32} = \frac{-ga\,\alpha A_1}{L_1' L_2'}$$

and

$$\alpha = \frac{(P_A - \rho g H)\gamma}{\rho V_o}.$$

Both equations differ only by the amplitude of the forcing function on the right hand side and it is apparent that they have oscillatory solutions.

Solving the homogeneous part yields the system's natural frequencies of oscillation:

$$\omega_0^{\pm} = \sqrt{\frac{a_1 \pm \sqrt{a_1^2 - 4a_2}}{2}}. \tag{12}$$

In the absence of forcing, the resonant and exhaust ducts oscillate about the position of equilibrium with the higher frequency (ω_0^+ in Figure 4, the one used for pumping), compressing and decompressing the air in between. The centre of mass itself oscillates back and forth as a unit with the lower frequency (ω_0^- in Figure 4). The forcing wave frequency is differentiated from the natural frequency of oscillation by using Ω and ω_0, respectively, for clarity.

Solving for V_o in equation 12 provides a tuning algorithm for the linearized model of the system in the absence of pumping (13). In Part II of this paper, this basic tuning algorithm is further analysed in the light of experimental data obtained in a wave tank with a model of the pump.

$$Vo_{Lin} = \frac{(P_A - \rho g H)\gamma}{\rho}\left[\frac{A_1}{L_1'\Omega^2 - g'} + \frac{A_c}{L_2'\Omega^2}\right]. \tag{13}$$

At resonance (i.e. $\Omega = \omega_b^+$, the "compression" natural frequency of oscillation), solutions for the resonant and exhaust ducts yield:

$$X_i = \frac{a_{3i}}{2\Omega(2\Omega^2 - a_1)}\left(t\cos(\Omega t) - \frac{\sin(\Omega t)}{\Omega}\right).$$

Water in the resonant duct and exhaust sides of the compression chamber oscillates up and down synchronously with an amplitude that increases linearly with time. The "bodily" oscillation of the centre of mass (ω_b^-) was neglected in this solution since it is likely to be damped out by the effect of pumping.

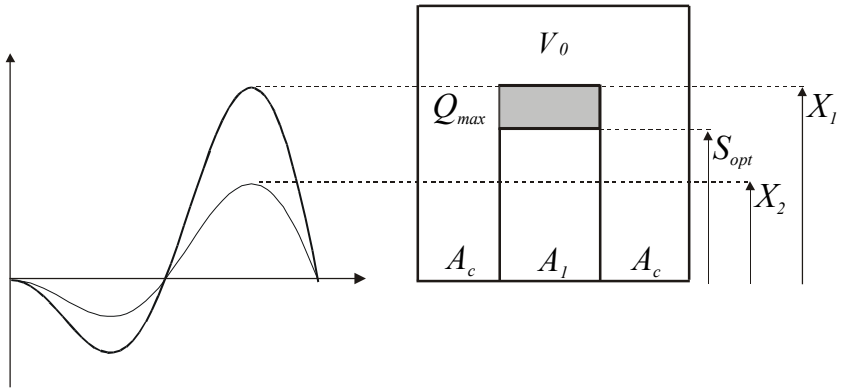

Figure 5. Linear solutions for the resonant and exhaust duct displacement used to estimate flow rate through the pump at resonance and the optimal sill height.

Without going into the actual dynamics of spilling, flow through the pump at resonance must be proportional to the difference between the increase of the oscillations in the resonant and exhaust ducts from one cycle to the next (Figure 5). This is because water can spill from the resonant to the exhaust duct only if there is a difference in level at the top of the cycle when the sill of the resonant duct is exceeded. The amount of water that would have to pass from one duct to the other in order to level the surface in both ducts at the top of the cycle corresponds to that which would have been pumped. An estimate of the attainable flow rate at resonance, for a given pump configuration, is then given by

$$Q_{max} = \frac{gaA_1A_c(L_2'\Omega^2 - \alpha(A_1 + A_c))}{2L_1'L_2'\Omega(2\Omega^2 - a_1)(A_1 + A_c)}. \tag{14}$$

This procedure also renders an estimate for the optimum height of the resonant duct sill above the equilibrium position in the compression chamber (S_{opt}). This is the height of the levelled surface above the equilibrium position in the compression chamber right after pumping:

$$S_{opt} = \frac{\pi g a A_1}{L_1'(A_1 + A_c)(2\Omega^2 - a_1)}. \tag{15}$$

While Q_{max} cannot give an accurate prediction of the flow rate through the pump because it was derived using the linearized equations, it can nevertheless provide valuable insight on how the various design parameters interact to determine pump efficiency. This information can be used to optimise the pump design. For example, it can be shown that Q_{max} increases for shorter resonant ducts when (14) is plotted against L_1 (see Czitrom, 1996). This increase occurs because the wave signal has to move a smaller mass of water and therefore is capable of pumping more efficiently. A plot of Q_{max} versus Ω (not presented here) shows that the system operates more efficiently at greater wave periods. In a similar way, it can be shown that Q_{max} increases for augmenting A_c, the compression chamber area. A detailed analysis of how the pump design can be optimised with cost benefit criteria, using equations 13 and (14), is given in Czitrom & Prado (In press).

SUMMARY AND CONCLUSIONS

A wave driven seawater pump, which has potential for various coastal management purposes such as aquaculture, flushing out of contaminated areas or the recovery of isolated coastal lagoons as breeding grounds is studied. Performance of the system is optimised by a novel tuning mechanism, which allows it to resonate at various wave frequencies.

An improved set of equations for the system, derived in this paper, takes into account the type of flow (laminar-turbulent) present in the ducts. A dimensional analysis of the pump equations shows that a proposed model operates similar to a full-scale system. The pump behaviour is basically linear and operates like a two mass-two spring system with relative small non-linear losses. The role of these losses is to limit the flow rate through the pump. Non-linear losses due to vortex formation at the duct mouths, can be further minimised, by improving the mouth design and thus optimising the pump performance. Formulae were derived, using the linearized pump equations, to estimate the volume of air needed for resonance, as well as the optimal sill height in the compression chamber. An estimate of the flow rate through the pump at resonance, given the various design parameters, can be used to optimise the pump design.

ACKNOWLEDGEMENTS

We wish to thank the John D. and Catherine T. MacArthur Foundation, through a grant from the Fund for Leadership Development, for their generous support in carrying out the work presented in this paper. Support was also provided by the Dirección General de Apoyo al Personal Académico (Projects IN-104193, 106694 and 107197) and the Instituto de Ciencias del Mar y Limnología (Project “Energía de Oleaje” No. 139), both from the National University of Mexico (UNAM). Support was also provided by CONACyT through project ‘Matemáticas no-lineales en la Física y en la Ingeniería, No 625427-E.

REFERENCES

Abramowitz, M. and I. Stegun, 1972. Handbook of Mathematical Functions, Cover Publications, USA.

Budall, K. and J. Falnes, 1975. A resonant point absorber of ocean-wave power. Nature, Vol. 256, pp. 478-479. (With corrigendum in Vol. 256, p.626).

Carey, D.J. and Z. Meratla, 1976. British Patent 1, 572, 086 (Granted 1980).

Czitrom, S.P.R. & Prado, E., In Press. Design optimisation of a Wave Driven Seawater Pump. Proc. 18th International Conference on Offshore Mechanics and Arctic Engineering.

Czitrom, S.P.R., 1996. Seawater pumping by resonance I, Proc. 2nd European Wave Power Conference, Lisbon, Portugal, ISBN 92-827-7492-9, pp. 366-370.

Czitrom, S.P.R., E. Prado, R. Godoy, R. Rodríguez and R. Peralta, 1996. Seawater pumping by resonance II, Proc. 2nd European Wave Power Conference, Lisbon, Portugal, ISBN 92-827-7492-9, pp. 324-328.

Czitrom, S.P.R., 1997. Wave Energy-Driven Resonant Seawater Pump. Journal of Offshore Mechanics and Arctic Engineering., Vol. 119, pp. 191-195.

Czitrom, S.P.R., Patent pending. Sintonizador para sistemas de extraccion de energía de oleaje que operan por resonancia. Solicitud de Patente Mexicana No. 933605.

Evans, D.V., 1982. Wave-power absorption by systems of oscillating surface pressure distributions, Journal of Fluid Mechanics, Vol. 114, pp. 481-499.

Evans, D.V., D.C. Jeffrey, S.H. Salter and J.R.M. Taylor, 1979. Submerged cylinder wave-energy device: theory and experiment. Applied Ocean Research. Vol. 1, pp. 3-12.

Falnes, J. and McIver, P., 1985. Surface wave interactions with systems of oscillating bodies and pressure distributions. Applied Ocean Research, Vol. 7, No. 4, pp. 225-234.

Isaacs, J.D., D. Castel and G.L. Wick, 1976. Utilization of the Energy in Ocean Waves. Ocean Engineering, Vol. 3, pp. 175-187.

Jonsson, I.G., 1980. A New Approach to Oscillatory Boundary Layers. Ocean Engineering, Vol. 7, pp. 109-152.

Justino, P.A.P., N.K. Nichols and A.F. Falcao, 1994. Optimal Phase Control of OWC's, Proc. European Wave Energy Symposium, Edinburgh, Scotland, ISBN 0-903640-84-8. pp. 145-149.

Knott, G.F. and J.O. Flower, 1979. Simulation studies of the basic non-linear effects of wave-energy conversion by an overtopping water-column. Energy Conversion, Vol. 19, pp. 59-69.

Knott, G.F. and J.O. Flower, 1980. Measurement of energy losses in oscillatory flow through a pipe exit. Applied Ocean Research, Vol. 2, No. 4, pp. 155-164.

Knott, G.F. and M.R. Mackley, 1980. Eddy-motions near plates and ducts induced by water waves and periodic flows. Philosophical Transactions of the Royal Society, Vol.. 294A, No. 1412, pp. 599-623.

Lighthill, J., 1979. Two-dimensional analyses related to wave-energy extraction by submerged resonant ducts. Journal of Fluid Mechanics, Vol. 91, part 2, pp. 253-317.

Malmo, O. and A. Reitan, 1985. Development of the Kvaerner Multiresonant OWC. Hydrodynamics of Ocean Wave-Energy Utilization. (Eds. D.V. Evans and A.F. Falcao). Springer-Verlag.

Masuda, Y., 1971. Wave-activated generator. Int. Coll. on the Expositions of the Oceans (Trans.), Bordeaux, France, March 1971.

McCormick, M.E., 1974. Analysis of a wave-energy conversion buoy. Journal of Hydronautics (AIAA), Vol. 8, No. 3, pp. 77-82.

Ohmi, M., M. Iguchi, T. Usui and H. Minami, 1980. Flow pattern and Frictional Losses in Pulsating Pipe Flow, Part 1: Effect of Pulsating Frequency on the Turbulent Flow Pattern. Bull. JSME, Vol. 23, No. 186, pp. 2013-2020.

Ohmi, M. and M. Iguchi, 1980a. Flow pattern and Frictional Losses in Pulsating Pipe Flow, Part 2: Effect of Pulsating Frequency on the Turbulent Frictional Losses. Bull. JSME, Vol. 23, No. 186, pp. 2021-2028.

Ohmi, M. and M. Iguchi, 1980b. Flow pattern and Frictional Losses in Pulsating Pipe Flow, Part 3: General Representation of Turbulent Flow Pattern. Bull. JSME, Vol. 23, No. 186, pp. 2029-2036.

Pérez, P., S.P.R. Czitrom, R. Peralta-Fabi and C. Treviño, 1996. Friction in Oscillating Flows. Proc. 2nd European Wave Power Conference, Lisbon, Portugal, ISBN 92-827-7492-9, pp. 375-380.

Raju, V.S., M. Ravindran and P.M. Koola, 1994. Experiences on a 150 KW wave energy pilot plant. Proc. European Wave Energy Symposium, Edinburgh, Scotland, ISBN 0-903640-84-8, pp. 277-282.

Rott, N., 1964. Theory of Time-Dependent Laminar Flows, In: High Speed Aerodynamics and Jet Propulsion, Princeton University Press, Vol. IV, pp. 395-438.

Salter, S.H., 1974. Wave Power, Nature, Vol. 249, pp. 720-724.

Sarmento, A.J.N.A. and A.F. de O. Falcao, 1985. Wave generation by an oscillating surface-pressure and its application in wave energy extraction. Journal of Fluid Mechanics, Vol. 150, pp. 467-485.

Sexl, T., 1930. Über den von E.G. Richardson entdeckten 'Annulareffekt', Z. Physik, Vol. 61, pp. 349-362.

Tjugen, K.J., 1994. Tapchan Ocean Wave Energy Project. Proc. European Wave Energy Symposium, Edinburgh, Scotland, ISBN 0-903640-84-8, pp.265-270.

Uchida, S., 1956. The Pulsating Viscous Flow Superposed on the Steady Laminar Motion of Incompressible Fluid in a Circular Pipe, Z. Angew. Math. Phys., Vol. 7, pp. 403-422.

White, F.M., 1991. Viscous Fluid Flow, Second Edition. McGraw-Hill International Editions, ISBN 0-07-069712-4, pp. 135-136.